DOE/ET-53088-278 IFSR #278

# Dynamical Transition to Second Stability in Auxiliary Heated Tokamaks

*G. Y. Fu, J. W. Van Dam,* and *M. N. Rosenbluth*
Institute for Fusion Studies
The University of Texas at Austin
Austin, Texas 78712

March 1989

# Dynamical Transition to Second Stability in Auxiliary Heated Tokamaks

G.Y. Fu, J.W. Van Dam, and M.N. Rosenbluth*
Institute for Fusion Studies
The University of Texas at Austin
Austin, Texas 78712
United States of America

**Abstract**

A simple transport model is developed to study the dynamic evolution of an auxiliary heated tokamak plasma during the transition to a high-beta, ballooning mode second-stable equilibrium. The effect of the ballooning mode stability on the transport is incorporated by prescribing an enhanced thermal diffusion in the unstable region. The resultant highly nonlinear transport equation is solved numerically as an initial value problem, and also analytically by means of boundary layer theory. In particular, the auxiliary heating power $P$ required for global transition of a flux-conserving tokamak plasma to the second stability regime is found to scale as $P\,\tau_E \propto \sqrt{\chi_{\max}}$, where $\chi_{\max}$ is the instability-induced thermal conductivity enhancement factor and $\tau_E$ is the confinement time in the ballooning stable regime.

*Current address: Department of Physics, University of California, San Diego, La Jolla, California 92093, USA

# 1 Introduction

It is well known that ideal ballooning modes can limit the beta value attainable in a tokamak operating in the usual first stability parameter regime, but that the existence of the theoretically predicted second stability regime could allow the possibility of high-beta operation. Various methods — e.g., highly energetic particles [1], cross-sectional shaping [2,3], current profile control [4], etc. — have been shown to be capable of stabilizing ballooning modes on individual flux surfaces for low values of the shear, thus providing a route by which to access the second stability regime.

In this work, we investigate the dynamical process by which a plasma confined in a tokamak can globally evolve toward second stability under the application of auxiliary heating. We employ a simple, self-consistent, one-dimensional transport model, with a large but finite anomalous thermal conductivity coefficient induced by ideal ballooning instability, and numerically solve for the time-dependent pressure profile, in the large aspect ratio limit. For the particular case of a flux-conserving plasma, we show that the problem of access to second stability can also be analytically recast in the form of a nonlinear laminar shock solution near the edge of the plasma. The numerical and analytical results predict a threshold heating power, as a function of the magnitude of the ballooning mode-enhanced transport, that is required for the plasma to attain a stable high-beta, steady-state profile.

The calculation in the present work follows, to some extent, from the ideal MHD ballooning mode transport model that was proposed by Connor, Taylor, and Turner [5] to explain the experimentally observed degradation of confinement in tokamaks with auxiliary heating. In their model, the time-independent pressure profiles corresponding to various applied powers were obtained, subject to INTOR transport scaling in the ballooning stable regime and to virtually infinite transport in the unstable regime (i.e., the thermal transport adjusts itself

such that the pressure gradient at each radial point does not exceed the marginal value corresponding to the low beta, first stability regime). Subsequently, Fu *et al.* [6,7] employed the same treatment to study tokamak confinement for the case of bifurcated marginal stability in which access to high-beta second stability is possible at low shear and found that globally second-stable equilibria can exist when the applied power exceeds a certain threshold. In the present work, the temporal evolution problem, with finite thermal transport in the unstable regime, is solved in order to show that the plasma can actually evolve self-consistently to a high-beta second-stable state with the application of sufficient power. Some preliminary results from this approach were presented at a workshop of the International School of Plasma Physics [8].

We should point out that the technique of balancing auxiliary heating power with enhanced heat conduction due to high-mode-number ballooning instabilities had been employed by Azumi *et al.* [9] to obtain two-dimensional flux-conserving equilibria that have marginally stable pressure profiles. The same authors [10] also considered the opposite case of very fast (compared to the confinement time) heating, as in a compression experiment: the plasma was allowed to heat up to high beta before the ballooning instability was turned on, after which the unstable regime adjusted itself self-consistently such that the entire equilibrium profile became second stable. However, this latter procedure does not yield a critical power estimate since it does not follow the self-consistent evolution to high beta stability, which is the problem that will be examined in the present work.

More recently, Sabbagh *et al.* [11] have undertaken a computational project in which a two-dimensional numerical equilibrium solver is iterated with a flux-surface-averaged transport code in order to calculate the heating required for access to second stability in a large-aspect-ratio tokamak. Their work shares the same basic approach as that of our investigation, and in a later section of this paper we will compare our results with theirs.

## 2 Theoretical Model

A self-consistent dynamical model of the plasma requires a description for both the pressure profile and the magnetic field. The evolution of the plasma profile will be described by the thermal transport equation

$$\frac{3}{2}\frac{\partial p}{\partial t} = \frac{1}{r}\frac{\partial}{\partial r}\left(r\chi\frac{\partial}{\partial r}p\right) + h \ . \tag{1}$$

Here, equal ion and electron temperatures ($T_i = T_e = T$), a constant density profile $n$, and large-aspect-ratio geometry are assumed. In Eq. (1), $p(r,t) = 2nT$ is the plasma pressure, and $\chi = (\chi_e + \chi_i)/2$ is the thermal conductivity. The auxiliary power deposition density $h$, which for simplicity, is also assumed to be constant in radius, is related to the auxiliary power $P$ by $P = 4\pi^2 R\int_0^a dr\, r\, h(r)$, with the ohmic power assumed to be negligibly small in comparison. Normalizing the radial coordinate $r$ to the minor radius $a$, the thermal conductivity $\chi$ to $\chi_0$ (its value in the ballooning stable regime), the time $t$ to $3a^2/2\chi_0$, and the pressure to $aB^2/(2\mu_0 R q_a^2)$ where $R$ is the major radius, $q_a$ is the safety factor at the edge, and $B$ is the toroidal magnetic field, we obtain the following normalized transport equation:

$$\frac{\partial \tilde{p}}{\partial \tau} = \frac{1}{x}\frac{\partial}{\partial x}\left(x\chi_n\frac{\partial}{\partial x}\tilde{p}\right) + H \tag{2}$$

with normalized radius $x$, conductivity $\chi_n$, time $\tau$, pressure $\tilde{p}$, and heating density $H$, where

$$H = \frac{64 P a \tau_E}{3\mu_0 I_p^2 R^2} \ . \tag{3}$$

Here $P$ is the total heating power, $\tau_E = 3a^2/16\chi_0$ is the confinement time in the stable regime, and $I_p = 2\pi a^2 B/\mu_0 R q_a$ is the plasma current ($\mu_0 = 4\pi \times 10^{-7}$).

Now we are ready to incorporate into the transport equation the anomalous transport induced by ideal ballooning instability. (This means that the thermal conductivity is retained, even while the electrical conductivity is taken to be so high that the plasma is collisionless.) Information about the stability of high-mode-number ideal ballooning modes is included

through a specification of the marginal stability boundary in terms of the pressure gradient parameter $\alpha = -(2\mu_0 R q^2/B^2)\partial p/\partial r$ and the shear $S = (r/q)\partial q/\partial r$. In the normalized variables we have $\alpha = -\tilde{q}^2 \partial \tilde{p}/\partial x$, with $\tilde{q}$ normalized to $q_a$. We will assume that the ballooning mode has some sort of supplemental stabilization at small values of the shear (e.g., provided by energetic particles, etc.). For simplicity we adopt a generic boundary as follows:

$$\alpha_{1,2}(S) = c_1 S \pm c_2 \left(S^2 - S_m^2\right)^{1/2} . \tag{4}$$

Note that the parameter $S_m$ is a measure of the supplemental stabilization and that $c_2$ is related to the width of the unstable region. Furthermore, within the unstable region, the thermal conductivity is taken to be enhanced by a factor proportional to the deviation beyond marginal stability, as follows:

$$\chi_n(\alpha, S) = 1 + \frac{4(\chi_{\max} - 1)}{(\overline{\alpha}_2 - \overline{\alpha}_1)^2} \left[\alpha - \alpha_1(S)\right] \left[\alpha_2(S) - \alpha\right] \tag{5}$$

where $\overline{\alpha}_{1,2}$ are the values of $\alpha_{1,2}(S)$ at the plasma edge and $\chi_{\max}$ controls the degree of transport enhancement. From Eq. (4) we have $\overline{\alpha}_{1,2} = c_1 S(a) \pm c_2 \sqrt{S^2(a) - S_m^2}$.

There is, however, a difficulty with the form given in Eq. (5) for the ballooning-enhanced thermal conductivity, which fortunately can be remedied by means of a numerical artifice. For lack of better information, we have assumed that in the second stability regime, the thermal conductivity returns to the same value it has in the first stability regime. This means that $\chi(\alpha, S)$ will decrease with increasing pressure gradient near the second stability marginal boundary $\alpha = \alpha_2(S)$. As a consequence, the coefficient of the highest derivative term, $\partial^2 \tilde{p}/\partial x^2$, in Eq. (2) when this equation is written in canonical form, this coefficient being

$$D = \chi_n + \left(\frac{\partial \chi_n}{\partial \alpha}\right) \alpha , \tag{6}$$

can vanish and even become negative as the solution approaches second stability. For $\chi_n$

having the form given in Eq. (5), $D$ is negative when $\alpha_0(S) < \alpha < \alpha_2(S)$, where

$$\alpha_0(S) = \frac{1}{3}\left\{\alpha_1(S) + \alpha_2(S) + \left([\alpha_2(S) - \alpha_1(S)]^2 + \alpha_1(S)\alpha_2(S) + \frac{3}{4}\frac{(\overline{\alpha}_2 - \overline{\alpha}_1)^2}{(\chi_{\max} - 1)}\right)^{1/2}\right\} . \quad (7)$$

As the singular point $D = 0$ is approached, the solution becomes discontinuous in nature (actually the shock-like discontinuity is exhibited by the gradient of the pressure); and when $D < 0$, numerical instability ensues. The instability manifests itself in very short wavelength oscillations such that the pressure gradient is effectively discontinuous from point to point in the numerical grid, with the oscillatory profile being different no matter how small the time increment is taken to be.

To prevent instability and resolve the discontinuity, we add a small *ad hoc* biharmonic term on the right-hand side of Eq. (2). The resultant equation is then given by

$$\frac{\partial \tilde{p}}{\partial \tau} = \frac{1}{x}\frac{\partial}{\partial x}\left(x\chi_n \frac{\partial}{\partial x}\tilde{p}\right) + H - \lambda \frac{1}{x}\frac{\partial}{\partial x}\left(x\frac{\partial^3}{\partial x^3}\tilde{p}\right) \quad (8)$$

where $\lambda$ is a small but nonzero positive constant. With this bi-Laplacian term, singular steepening of the pressure gradient profile is avoided. To stabilize this instability at the shortest wavelengths, we approximately require $\lambda > (-D)_{\max}(\Delta x)^2$, where $\Delta x$ is the spatial gridsize in the numerical solution of Eq. (8). On the other hand, we want $\lambda \ll 1$ so that the dispersive effect of this biharmonic term on the bulk of the plasma is very small. As long as $\lambda \ll 1$, the biharmonic term is important only in a narrow transition layer near the plasma edge, whose width is proportional to $\sqrt{\lambda}$ and within which the pressure gradient changes rapidly but not discontinuously. We will show later that our analytic results have a well-defined limit as $\lambda \to 0$. We will also find that the numerical results are relatively insensitive to the exact value of $\lambda$, as long as this coefficient is judiciously chosen to satisfy the two previous inequalities. Physically, this biharmonic term can be said to provide a scale-selective "smoothing" effect on the shock-like discontinuity by dissipating energy at very short wavelengths.

Incidentally, artificial dissipation mechanisms represented by bi-Lapacian (or higher order) terms, either linear (as in Eq. (8)) or nonlinear in form, have long been used in fluid dynamics [12,13] as an automatic means to handle shock-type solutions in numerical calculations. Usually such terms are generically referred to as hyper-viscosity (or pseudo-viscosity). To cite a few examples from recent plasma physics literature, Strauss [14], in a study of the dynamo effect in fusion plasmas, derived such a term in the mean-field Ohm's law modified by turbulent fluctuations; this turbulence-enhanced resistive dissipation has been dubbed "hyper-resistivity." Hogan [15], in a model for turbulent current penetration, introduced a "hyper-viscosity" term in the poloidal field diffusion equation. It has been suggested [16] that the $\lambda$ term in Eq. (8), representing "hyper thermal conductivity," could presumably be constructed from renormalized turbulence theory.

We still need to determine the safety factor $q$ profile, which contains the magnetic field information since $q(r) = rB/RB_p(r)$. We consider two limiting cases: one is the flux-conserving tokamak (FCT) case, and the other is the non-flux-conserving case. For the flux-conserving case, the heating is rapid compared to the magnetic skin time, so that the poloidal field is constant and the $q$ profile is invariant in time. For the numerical results reported in this paper, we took $q = 1 + 2x^2$. Note that $S = 1.33$ at the plasma edge for this particular choice of profile.

On the other hand, for the flux non-conserving case, we take the heating to be slow compared to the skin time. Then $q(x, \tau)$ can be self-consistently determined from Ohm's law and Ampere's equation:

$$J_z = \frac{1}{r}\frac{\partial}{\partial r} r\, B_\theta = \sigma E_z \ , \tag{9}$$

where $J_z$ is the toroidal current density, $E_z$ is the toroidal electrical field, and $\sigma$ the electrical conductivity. Using the Spitzer resistivity, we have $\sigma \propto p^{3/2}$ for uniform density. Then

Eq. (9) can be written [5] in normalized form as follows:

$$\frac{\partial}{\partial x}\left(\frac{x^2}{\tilde{q}}\right) = \frac{x\tilde{p}^{3/2}}{\int_0^1 x\tilde{p}^{3/2}dx} \ . \tag{10}$$

Numerical results for both cases will be presented in the next section. The analytical theory of Sec. 4, however, will be mainly relevant to the flux-conserving case.

# 3 Numerical Results

Equation (8) was integrated as an initial value problem in time with an implicit scheme, and as a boundary value problem in radius with a centered difference scheme. The boundary conditions employed here were $\partial\tilde{p}/\partial x = 0$ and $\partial^3\tilde{p}/\partial x^3 = 0$ at $x = 0$ (magnetic axis), and $\tilde{p} = 0$ and also $\partial^2\tilde{p}/\partial x^2 = 0$ at $x = 1$ (plasma edge). Since the thermal conductivity $\chi_n$ is a nonlinear function of the pressure, it was evaluated at the preceding time step in the implicit scheme, which approximation is reasonably accurate for small time increments.

The numerical stability of the finite difference form of the transport equation, including the hyperviscosity $\lambda$ term, can be examined in the usual way with von Neumann analysis [12]. Take $u(x,\tau) = \partial\tilde{p}/\partial x$ as the dependent variable for convenience, and regard the coefficients of the differential equation as approximately constant in a small region (since instability, when it occurs, appears as localized rapid oscillations). Then set $u_j^n = \xi^n \exp[ik(j\Delta x)]$, where the indices $n$ and $j$ denote time step and spatial grid point, respectively, and solve for the amplification factor $\xi$:

$$\xi \cong [1 + F\,\Delta\tau(D + \lambda F)]^{-1} \ . \tag{11}$$

Here, $D = \chi_n(u) + u(\partial\chi_n/\partial u)$ is evaluated at the preceding time step $n-1$, and $F(k,\Delta x) = 4\sin^2(k\Delta x/2)/(\Delta x)^2$. Stability requires $|\xi| \leq 1$. When $D > 0$, the solution is unconditionally stable, characteristic of the implicit scheme. In regions where $D$ is negative, the solution can be unstable. However, instability at the shortest wavelengths, where $F = 4/(\Delta x)^2$, is

avoided by having the value of $\lambda$ be such that

$$\lambda \geq c(\Delta x)^2(-D)_{\max}/4 \ , \tag{12}$$

with $c \geq 1$ a constant. Wavelengths larger than $N(\Delta x)$, with $N \approx \pi/\sin^{-1}(1/\sqrt{c})$, may be unstable where $D$ is negative; for these unstable wavelengths, $\xi$ remains finite as long as $\Delta\tau < 4\lambda/[(-D)_{\max}]^2$. In our computations reported here, typically we had $\Delta x = 1/400$ and $\Delta\tau \leq 10^{-5}$, with $(-D)_{\max}$ several times $\chi_{\max}$ and $\lambda \approx 10^{-3}\chi_{\max}$, thus satisfying these inequalities.

To save computer time, we began the integration (at time $\tau = 0$) with a nonzero pressure profile that lies entirely in the first stability region and that satisfies the time-stationary version of Eq. (8). Such solutions can, in fact, be written in analytic closed form and will be given in Eq. (19). One could, alternatively, begin with zero pressure. However, the amount of *energy* that is then required to heat the plasma to our initial solution does not change the value of the critical *power*. Hence, to save time, we start from an initially non-zero, but self-consistent, profile. We also stop the integration as soon as the profile has completely gone through the unstable zone and entered second stability, since thereafter the profile will eventually asymptote to a time-independent final state, which again is irrelevant to the calculation of the power threshold for access. (This time-asymptotic tendency was checked with longer runs in a few cases.)

Figure 1 shows the time evolution of the pressure profile for the flux-conserving case. Recall that the safety factor profile, which is constant in this case, was taken to be $q = 1+2x^2$. The sequence shown in Fig. 1 was obtained with $H = 30$, $\chi_{\max} = 20$, $\lambda = 0.025$, $S_m = 0.8$, $c_1 = 0.8$, and $c_2 = 0.4$. The dashed curve is the generic ballooning stability boundary of Eq. (4), plotted in the $(-\partial\tilde{p}/\partial x, x)$ space. Inside this dotted curve the ballooning mode is unstable, whereas the region below the unstable regime is the first stability regime and the region above it is the second stability regime. Initially, for small heating power, the

plasma profile (solid curve $a$) is completely in the first stability regime. At time $\tau = 0$, we increased the heating power to $H = 30$, which is above the critical threshold power; then the plasma pressure begins to increase, as does the pressure gradient. After a time $\tau = 0.1$ has passed, a large part of plasma (curve $b$) has entered the ballooning unstable region. At time $\tau = 0.15$, the profile (curve $c$) has entered the second stability regime at all radii except near the plasma edge. Finally, at $r = 0.175$, the entire plasma profile (curve $d$) is in the second regime, although it is still evolving to higher pressure gradients. Eventually, the profile attains a globally second-stable equilibrium that no longer changes in time. A similar case is shown in Fig. 2, plotted in $(S, \alpha)$ variables.

Figure 3 shows the result when the power is not sufficiently large: the pressure profile reaches a steady state, but the profile is not everywhere in the stable domain. Figure 3 was obtained with $H = 21$, which is just below the critical value $H_{\rm crit} = 21.5$. The other parameters here are the same as in Fig. 1. (The labels $A$, $B$, and $C$ will be used in the discussion of Sec. 4.2.)

By varying the applied power, one finds the critical value below which such access becomes impossible. Approximately, we find from the numerical results (for $S_m = 0.8 = c_1$ and $c_2 = 0.4$, as in Fig. 1) the following scaling relationship for the critical heating power $H_{\rm crit}$ as a function of the transport enhancement factor $\chi_{\rm max}$ in the flux-conserving case:

$$H_{\rm crit} \cong 5\sqrt{\chi_{\rm max}} \ . \tag{13}$$

The numerical results themselves will be presented in Fig. 7, where they are compared to the analytical results of Sec. 4.

Choosing an appropriate value for $\lambda$ is a subtle issue, as has been remarked earlier. On the one hand, $\lambda$ must be large enough to overcome the negative diffusion-induced numerical instability and to maintain numerical accuracy; on the other hand, $\lambda$ must be small enough to make our results nearly independent of the precise value of $\lambda$. We found, within numerical

error, that $H_{\rm crit}$ does slightly depend on $\lambda$ for finite values of $\lambda$. However, as $\lambda$ goes to zero, $H_{\rm crit}$ saturates to a limiting value. In obtaining the scaling given in Eq. (13), we chose $\lambda$ as

$$\lambda = 1.25 \times 10^{-3} \chi_{\rm max} \ . \tag{14}$$

In the next section we will show that as long as $\lambda$ is small enough, $H_{\rm crit}$ does not depend on $\lambda$.

We have also studied the non-FCT case. Here the $q$ profile is determined in terms of $\tilde{p}$ from Eq. (10), and our transport equation, Eq. (8), has to be solved in conjunction with Eq. (10). Shown in Fig. 4 are the numerical results for $H_{\rm crit}$ versus $\chi_{\rm max}$, plotted for the parameters of $S_m = 1.2$, $c_1 = 0.8$, $c_2 = 0.4$, and $\lambda = 2 \times 10^{-4} \chi_{\rm max}$. For large $\chi_{\rm max}$ values, the numerical results approximately fit the scaling relationship

$$H_{\rm crit} = 3.7 \chi_{\rm max} \ . \tag{15}$$

Notice that in the flux non-conserving case, a linear scaling with $\chi_{\rm max}$ holds instead of the square root scaling for the flux-conserving case. In the next section we will derive these scalings analytically in the small $\lambda$ limit.

Before leaving this section, we point out a few features of the numerical results that can be described analytically. First of all, the boundary conditions imply that the pressure profile has the following general behavior near the magnetic axis ($x = 0$) and near the edge of the plasma ($x = 1$):

$$\tilde{p}(x) = \begin{cases} \tilde{p}(0) + \dfrac{1}{2} x^2 \tilde{p}''(0) & \text{for } x \ll 1 \\ \\ (x-1)\tilde{p}'(1) + \dfrac{1}{3!}(x-1)^3 \tilde{p}'''(1) & \text{for } x \lesssim 1 \ , \end{cases} \tag{16}$$

where primes denote radial derivatives. This information can be translated to the profiles as plotted in the $(S, \alpha)$ variables that are relevant to high-mode-number ballooning stability. For a non-flux-conserving profile, this is accomplished with the use of Eq. (10), which can

be rewritten in terms of the global shear $S$ as

$$S = 2 - \frac{\tilde{q}\,\tilde{p}^{3/2}(x)}{\int_0^1 dx\, x\, \tilde{p}^{3/2}(x)} \,. \tag{17}$$

Note that $S \to 2$ at the edge of a non-FCT plasma in the cylindrical approximation. Since $\alpha'/\alpha = 4/x + (2/x)(S-2) \to 4$ at $x = 1$, we find

$$\frac{dS}{d\alpha} \propto [1 - \alpha(x)/\alpha(1)]^{1/2} \tag{18}$$

near the plasma edge, whereas by expanding for $x \ll 1$, we find $S \propto \alpha^2$ near the magnetic axis. These results, since they follow from only the boundary conditions and the equation for $q(r)$, are independent of the thermal conductivity profile that is chosen. Similar results can be obtained for the FCT case, depending on the assumed form for $q(r)$.

Secondly, the energy confinement time $\tau_E$, defined as $\tau_E = \varepsilon/(P - d\varepsilon/dt)$ where $\varepsilon = \frac{3}{2}\int d^3r\, p(r)$ is the energy content of the plasma (in unnormalized variables), is a function of time during the evolution of the profile under the application of auxiliary heating. As the profile enters the ballooning unstable zone, $\tau_E$ will decrease; if the auxiliary power is sufficient to heat the plasma into second stability, then eventually $\tau_E$ recovers. Carreras [17] has recently suggested that such experimentally observed improvement of confinement with increasing beta will be a useful manifestation of access to high-beta stability. This regime might thus better be termed "second transport," rather than second stability.

Once the plasma has settled down to a globally stable profile, the steady-state confinement time can be easily calculated. In the time-stationary limit, Eq. (8) has an exact solution:

$$\tilde{p}(x) = \frac{H}{4}(1 - x^2) + \frac{1}{2}\lambda H \left[\frac{\cosh\left(x/\sqrt{\lambda}\right)}{\cosh\left(1/\sqrt{\lambda}\right)} - 1\right] \,. \tag{19}$$

This solution explicitly shows that for $\lambda \ll 1$, the $\lambda$-dependent terms modify the profile only near the plasma edge (i.e., for $|x - 1| < \sqrt{\lambda}$) and then only for third and higher derivatives

of the pressure. With this solution, the confinement time (unnormalized) in a stable regime is

$$\tau_{E_0} = \frac{3a^2}{16\chi_0}\left\{1 - \lambda\left[4 - 8\sqrt{\lambda}\,\tanh\left(1/\sqrt{\lambda}\right) + 8\lambda\left(1 - \mathrm{sech}\left(1/\sqrt{\lambda}\right)\right)\right]\right\} . \qquad (20)$$

Since $\lambda \ll 1$, this yields the usual result (viz., the first term), which becomes $\tau_{E_0} \cong 1/8$ in normalized units.

Incidentally, we note that the form of the thermal transport equation prevents the development of regions of negative pressure. It can be seen that even if local minima in $\tilde{p}(x)$ develop during the time evolution, it is not possible for the pressure to become negative at these points. At a local minimum, we have $\partial\tilde{p}/\partial x \ll 1$, and hence the "effective" diffusion coefficient is positive, $D \cong \chi_n + (\partial\chi_n/\partial\tilde{p}')\,\tilde{p}' > 0$. Furthermore, at a minimum, $\partial^2\tilde{p}/\partial x^2 > 0$ and $\partial^4\tilde{p}/\partial x^4 < 0$, and therefore the transport equation implies $\partial\tilde{p}/\partial\tau > 0$, so that the pressure cannot become negative here.

# 4 Analytic Theory

## 4.1 Analysis of Edge Behavior

In Figs. 1 and 2 it can be observed that the last part of the pressure profile to make the transition into second stability occurs near the edge of the plasma, where the enhancement of the thermal conductivity is maximum. Furthermore, the numerical results show that if the heating power is less than some critical value, the plasma pressure assumes a time-independent profile that has not achieved access into the second stability regime. Therefore, in this section, let us consider the steady-state behavior of the thermal transport equation, near the plasma boundary.

To begin with, integrate Eq. (8) once to obtain the flux equation for the thermal energy density:

$$\frac{\partial}{\partial\tau}\int_0^x dx' x'\tilde{p}(x',t) = x\chi_n\frac{\partial}{\partial x}\tilde{p} + \frac{1}{2}x^2 H - \lambda x\frac{\partial^3}{\partial x^3}\tilde{p} . \qquad (21)$$

(Note that the quantity $H$ in Eq. (21) is to be replaced by $\langle H \rangle = \int_0^x dx\, x\, H(x) \Big/ \int_0^x dx\, x$ if the heating power varies across the plasma radius; with this change in interpretation, the analysis of this section applies equally well to cases with nonuniform heating.) Now explore the possibility of the existence of a stationary solution ($\partial/\partial t = 0$), near the edge of the plasma. Change the radial coordinate to $\xi = 1 - x$ (with $|\xi| \ll 1$), fix the shear at its edge value $S = S(x = 1) =$ constant, and define $y = \partial\tilde{p}/\partial\xi$ as the independent variable. Equation (21) can then be rewritten as

$$\lambda \frac{d^2 y}{d\xi^2} = -\frac{\partial}{\partial y} V(y) , \tag{22}$$

with

$$V(y) = \frac{1}{2} H y - \frac{1}{2} y^2 - \int_{\overline{\alpha}_1}^{y} dy' y' \left[\chi_n(y') - 1\right] . \tag{23}$$

Equation (22) has the form for the one-dimensional equation of motion for a particle of "mass" $\lambda$ in a "potential" $V(y)$. We pursue this analogy, adopting techniques that have been used by Sagdeev [18] and others [19] to study laminar shock waves. The structure of the quasi-potential $V(y)$ determines the nature of the nonlinear solutions. The form for the potential $V(y)$ is shown in Fig. 5 for several values of the power $H$. As the power is increased, two peaks appear, with a valley in between. The height of the peak at large $y$ increases with the applied power, whereas the height of the peak at small $y$ remains nearly constant. In particular, we desire a bounded solution for the "coordinate" $y$ that extends in "time" $\xi$ so as to connect the large $y$ (i.e., second-stable, large $|\nabla p|$) solutions in the interior of the plasma smoothly to a non-second-stable, small-$y$ solution at the edge of the plasma. Note that the "velocity" $dy/d\xi$ is zero both at the edge of the plasma ($x = 1$) by virtue of the boundary conditions and at the point ($x \lesssim 1$) where this laminar edge solution joins onto the interior second stable solution. In the language of the motion of a ball in a potential, we want a solution for which a ball (which starts from rest) rolls down the hill from the peak

at large $y$ and goes no farther than the peak at small $y$. This desired motion of a ball is possible only if the height of the peak at large $y$ is the same or lower than the peak at small $y$. When the peak at large $y$ is higher than the peak at small $y$, a ball starting from rest on the large-$y$ peak will roll over the peak at small $y$, continuing leftward. A bounded solution is then not possible, which implies that the stationarity assumption is no longer valid: the plasma energy content will increase in time, and the solution for the pressure will evolve so as to be eventually everywhere lying in the large-$|\nabla p|$ regime of second stability. Therefore, the critical heating power, i.e., the heating power below which the plasma cannot gain access to the second regime, is determined by the condition that the two peaks of the potential have equal height.

We now proceed to quantify this condition for the critical heating power. Let $y_a, y_b$, and $y_c$ designate the locations of the small-$y$ peak, the valley, and the large-$y$ peak of the quasi-potential $V(y)$. These three locations are found as the solutions of $\partial V/\partial y = 0$, which equation can be written as

$$2y\,\chi(y) = H\ . \tag{24}$$

Note that for the quasi-potential to have two peaks, the normalized heating power $H$ must lie in the range $H_{\min} < H < H_{\max}$, where

$$H_{\min} = 2\overline{\alpha}_2 \tag{25}$$

$$H_{\max} = \frac{16}{27}\frac{(\chi_{\max}-1)}{(\overline{\alpha}_2-\overline{\alpha}_1)^2}\left\{(\overline{\alpha}_1+\overline{\alpha}_2)\left[(\overline{\alpha}_2-\overline{\alpha}_1)^2\left(1+\frac{9/8}{\chi_{\max}-1}\right)-\frac{1}{2}\,\overline{\alpha}_1\overline{\alpha}_2\right]\right.$$

$$\left.+\left[(\overline{\alpha}_2-\overline{\alpha}_1)^2\left(1+\frac{3/4}{\chi_{\max}-1}\right)+\overline{\alpha}_1\overline{\alpha}_2\right]^{3/2}\right\}. \tag{26}$$

(The obvious condition $H_{\max} > H_{\min}$ leads to the mild constraint of $\chi_{\max} > 1+(\overline{\alpha}_2-\overline{\alpha}_1)/4\overline{\alpha}_2$, which is satisfied as long as $\chi_{\max} > 1.25$.) We are interested in evaluating the critical power,

$H_{\rm crit}$, which is characterized by the two peaks being of equal height:

$$V(y_a) = V(y_c) \qquad \text{when} \qquad H = H_{\rm crit} \ . \tag{27}$$

In view of the fact that $y_c > \overline{\alpha}_2$, we immediately find $y_c = \frac{1}{2} H$ and

$$V(y_c) = \frac{1}{8} H^2 - \int_{\overline{\alpha}_1}^{\overline{\alpha}_2} dy\, y\, [\chi(y) - 1] \ . \tag{28}$$

The preceding threshold condition can then be viewed as an equation for the critical power as a function of the quantity $y_a$: i.e., $H_{\rm crit} = F(y_a)$, where

$$F(y_a) = 2y_a + \left\{ 8 \int_{y_a}^{\overline{\alpha}_2} dy\, y\, [\chi(y) - 1] \right\}^{1/2} \ . \tag{29}$$

This expression can be used to eliminate $H$ in Eq. (24), which then yields the equation that determines $y_a$:

$$2y_a\, \chi(y_a) = F(y_a) \ . \tag{30}$$

For given values of $\overline{\alpha}_1$, $\overline{\alpha}_2$, and $\chi_{\rm max}$, Eq. (30) can be solved for $y_a$, which, when substituted into Eq. (29), gives the corresponding value for the critical power. Note that for the specific form for $\chi(y)$ assumed in Eq. (5), we can explicitly write Eq. (30) as follows:

$$\frac{4(\chi_{\rm max} - 1)}{(\overline{\alpha}_2 - \overline{\alpha}_1)^2}\, y_a^2 (y_a - \overline{\alpha}_1)^2 = \frac{1}{2} (\overline{\alpha}_2 - y_a)^2 - \frac{2}{3} (2\overline{\alpha}_2 - \overline{\alpha}_1)(\overline{\alpha}_2 - y_a) + \overline{\alpha}_2 (\overline{\alpha}_2 - \overline{\alpha}_1) \ . \tag{31}$$

A limit of special interest is that of large instability-induced enhancement of the thermal conductivity, $\chi_{\rm max} \gg 1$. In this limit, we have $y_a \to \overline{\alpha}_1$ approximately, and from Eq. (29) we find

$$H_{\rm crit} \cong \sqrt{8} \left\{ \int_{\overline{\alpha}_1}^{\overline{\alpha}_2} dy\, y\, [\chi(y) - 1] \right\}^{1/2} \ . \tag{32}$$

In particular, note the scaling $H_{\rm crit} \propto \sqrt{\chi_{\rm max}}$ that holds in this limit. For the specific form for $\chi$ given in Eq. (5), the coefficient of proportionality can be given as

$$H_{\rm crit} / \sqrt{\chi_{\rm max}} = \left[ \frac{8}{3} (\overline{\alpha}_2^2 - \overline{\alpha}_1^2) \right]^{1/2} \longrightarrow 2.2 \ , \tag{33}$$

where we evaluated the coefficient for the parameters of Fig. 1.

This edge analysis reproduces the $\chi_{\max}^{1/2}$ scaling of $H_{\text{crit}}$ that was obtained numerically. However, the theoretically predicted proportionality coefficient is approximately one-half of the value for the coefficient that was found numerically, which is given in Eq. (13). In the next section we will give a refined theory to explain this discrepancy.

## 4.2 Boundary Layer Analysis

Here we will develop a refined theory to resolve the discrepancies between the numerical results of Eq. (13) and Eq. (15) and the analytic scaling of Eq. (33). In particular, for the flux-conserving case we found a factor of two difference in the proportionality coefficient for the parameters of Fig. 1. The problem is more serious for the flux non-conserving case, where the discrepancy lies not merely in the coefficient but in the scaling. Therefore, a unified analytic theory is called for.

We also are motivated by the numerical results for the profile of the marginal steady-state equilibrium just before transition to second stability regime. Shown in Fig. 3 is a typical marginal profile of $y$ versus $x$. Notice we can characterize the profile $y(x)$ in terms of three parts: namely, the inner part (labeled $A$) that lies in the stable regime $0 < x < x_1$; the intermediate part (labeled $B$) with $x_1 < x < x_2$, which is a boundary layer in which $y$ changes very rapidly; and finally the outer part (labeled $C$) that lies in the unstable regime with $x_2 < x < 1$, in which $y$ varies slowly. Observe that the boundary layer for the marginal steady state is located at $x = x_1 < 1$, rather than at $x = 1$, as was assumed in the edge analysis of Sec. 4.1. Here we will show that the location of the boundary layer is very crucial to the value of the coefficient of the $H_{\text{crit}}$ scaling and that the assumption of the boundary layer being at the edge in the analysis of Sec. 4.1 is exactly the reason for the occurence of the discrepancies.

Here we will solve the steady-state version of Eq. (8) in the unstable boundary layer

by the quasi-potential method, and then match this boundary layer solution to the stable solution in the interval labeled $A$. To begin with, Eq. (8) with $\partial/\partial\tau = 0$ can be integrated once in $x$ and rewritten in the following form:

$$\lambda \frac{d^2y}{dx^2} = \chi_n(y,x)\, y - \frac{1}{2} Hx \ . \tag{34}$$

Since $\chi_n = 1$ in the stable regime, the solution of Eq. (34) in interval $A$ can be easily obtained as

$$y = \frac{1}{2} Hx + \left(y_1 - \frac{1}{2} Hx_1\right) \frac{\sinh(x/\sqrt{\lambda})}{\sinh(x_1/\sqrt{\lambda})} \tag{35}$$

where the boundary conditions $y(0) = 0$ and $y''(0) = 0$ have been applied. The undetermined quantity $y_1 = y(x_1)$ in Eq. (35) is the value of $y$ at the point $x = x_1$ on the second stability boundary. Then the derivative of $y$ at this point is

$$y'_{x_1^-} = \frac{1}{2} H \left[1 - \frac{(x_1 - 2y_1/H)}{\sqrt{\lambda}\, \tanh\left(x_1/\sqrt{\lambda}\right)}\right] \ . \tag{36}$$

In interval $B$, since $y$ varies rapidly as a function of $x$, Eq. (34) can be treated as a boundary layer problem. That is to say, because $\lambda \ll 1$, we can neglect the $x$ variation on the right-hand side of Eq. (34). Then the solution can be obtained with the quasi-potential analysis of Sec. 4.1, except that now the boundary layer is located at $x = x_1 < 1$ instead of at $x = 1$. Using quadrature, we obtain the result

$$y'^2_{x_1^+} - y'^2_{x_2} = \frac{2}{\lambda} \left\{ \int_{y_2}^{y_1} dy'\, y' \left[\chi_n(y', x_1) - 1\right] + \frac{1}{2}\left(y_1^2 - y_2^2\right) - \frac{1}{2} Hx_1(y_1 - y_2) \right\} \ . \tag{37}$$

In Eq. (37), $y_2$ is the value of $y(x)$ at $x = x_2$; this point represents the location of the transition from the boundary layer ($B$), in which $y$ varies rapidly, to the interval ($C$) near the plasma edge, within which $y$ hardly changes. We will not pursue the solution in this latter interval, since it turns out to have little effect on the final result. We simply make the reasonable approximation $y_2 \approx y_{\text{first}}(x_1) = \tilde{q}^2(x_1)\alpha_1[S(x_1)]$, where $y_{\text{first}}$ means the first stability boundary, i.e., the low pressure gradient portion of the marginal stability curve. Also, we neglect the derivative $y'_{x_2}$ in Eq. (37), since $|y'_{x_2}| \ll |y'_{x_1}|$ by inspection.

From the matching condition $y'^2_{x_1^-} = y'^2_{x_1^+}$ with Eqs. (36) and (37), we then obtain an expression for the power $H$:

$$H = \frac{\tanh\left(x_1/\sqrt{\lambda}\right)}{\left[x_1 - \sqrt{\lambda}\,\tanh\left(x_1/\sqrt{\lambda}\right)\right]}\left\{2\delta y_2 + \left[4(\delta^2-1)y_2^2 - 4y_1^2\,\mathrm{csch}^2\left(x_1/\sqrt{\lambda}\right) + 8\int_{y_2}^{y_1} dy\, y\,[\chi(y,x_1)-1]\right]^{1/2}\right\}, \quad (38)$$

with

$$\delta = \frac{x_1(1-y_1/y_2)\tanh^2\left(x_1/\sqrt{\lambda}\right) + (y_1/y_2)\left[x_1 - \sqrt{\lambda}\,\tanh\left(x_1/\sqrt{\lambda}\right)\right]}{\left[x_1 - \sqrt{\lambda}\,\tanh\left(x_1/\sqrt{\lambda}\right)\right]\tanh\left(x_1/\sqrt{\lambda}\right)}\,. \quad (39)$$

For the specific form for the thermal conductivity given in Eq. (5), we have

$$\int_{y_2}^{y_1} dy\, y\,[\chi(y,x_1)-1] = \frac{\tilde{q}_1^4(\chi_{\max}-1)}{3(\overline{\alpha}_2-\overline{\alpha}_2)^2}(y_1-y_2)^3(y_1+y_2) \quad (40)$$

where $\tilde{q}_1$ is the safety factor at $x = x_1$ (normalized to its edge value $q_a$). Equation (38) can be regarded as a dispersion relation for a steady state bounded by the ballooning unstable region. For specific values of $\chi_{\max}$ and the power $H$, the position of the boundary layer, $x_1$, can be determined through Eq. (38). In general, $x_1$ is a function of the parameters $\lambda, H$, and $\chi_{\max}$, the $q$ profile, and also the marginal stability boundary. In the case of a flux-conserving tokamak, the stability boundary in $(y,x)$ space does not change, since $q(x)$ has a fixed functional form. Then, from Eq. (38), $H$ is only a function of $x_1$, for given values of $\lambda$ and $\chi_{\max}$. Shown in Fig. 6 is $H$ plotted as a function of $x_1$, for the parameters of Fig. 1 (viz., $\lambda = 0.025$ and $\chi_{\max} = 20$). Notice that there is a maximum at $x_1 = x_{1,\max} \cong 0.74$. For $H < H(x_{1,\max})$, we have two roots for $x_1$. The larger root for $x_1$ is inaccessible for physical reasons. Then, from Fig. 6, we observe that as $H$ increases, $x_1$ (the smaller root) also increases; i.e., the boundary layer for the bounded steady state shifts toward the edge of the plasma. When $H > H(x_{1,\max})$, a bounded state no longer exists. Thus, the critical power is $H_{\mathrm{crit}} = H(x_{1,\max})$. For the particular case of Fig. 6, we obtain $H_{\mathrm{crit}} \cong 18.2$; this is equivalent to $4.1\sqrt{\chi_{\max}}$, which compares well with the numerical result, given in Eq. (13).

Equation (38) can be simplified considerably by noting that $x_1/\sqrt{\lambda} \gg 1$, so that to a good approximation it becomes

$$H \cong \frac{2\delta y_2 + \sqrt{4(\delta^2-1)y_2^2 + 8\int_{y_2}^{y_1} dy\, y[\chi_n(y,x_1)-1]}}{x_1 - \sqrt{\lambda}} \tag{41}$$

with

$$\delta = \frac{x_1 - \sqrt{\lambda}\, y_1/y_2}{x_1 - \sqrt{\lambda}} . \tag{42}$$

Note that in the limit where $x_1 = 1$ and $\lambda \to 0$, Eq. (41) reduces to Eq. (29) exactly if we let $y_2 = y_a$. Therefore the critical power determined here by $H = H(x_{1,\max})$ reproduces the results of the edge quasi-potential analysis of Sec. 4.1 in the $\lambda = 0$ and $x_{1,\max} = 1$ limit. In Fig. 6, we also plotted the function $H(x_1)$ for $\lambda = 0$. The value of this curve at the plasma edge corresponds to the critical power of the edge analysis, given by Eq. (29). Figure 7 compares the numerical results with the analytic results of Sec. 3 from both the edge analysis of Sec. 4.1 and the boundary layer theory of this section. It is evident that the boundary layer analysis provides a substantial improvement over the edge analysis in terms of agreement with the numerical results.

For the flux non-conserving case, the procedure to obtain $H_{\rm crit}$ is more subtle, since now the safety factor profile $\tilde{q}(x)$ is related to the pressure profile $\tilde{p}(x)$, and Eq. (8) has to be solved self-consistently in conjunction with Ampere's law, Eq. (10). As $H$ increases, the $\tilde{p}(x)$ profile tends to peak near the center of the plasma, and as a result the stability boundary in $(y,x)$ space will change accordingly; in particular, the unstable regime will be enlarged and will extend toward small minor radii. Numerically, we find that the net effect is to decrease the value of $x_1$ in Eq. (38). By balancing terms in Eq. (8), we can find roughly that $x_1$ scales as $x_1 \propto 1/\sqrt{H}$ for the marginal steady-state solution. Then, from Eq. (41), we obtain a linear scaling: $H_{\rm crit} \propto \chi_{\max}$ for the flux non-conserving case. This linear scaling tends to agree with the numerical results of Fig. 4 and Eq. (15). To determine the coefficient for

this linear scaling, one would have to solve for the entire profile $\tilde{p}(x)$ self-consistently; this procedure is quite involved and not illuminating, so we will not pursue it here farther.

Incidentally, the effect of hot particle stabilization (or of whatever supplemental stabilization is assumed) on $H_{\rm crit}$ may be implicitly seen through the dependence on $S_m$ in the stability boundary in Eq. (38). For example, the presence of hot particles [1] tends to raise the nadir point $S = S_m$ of the stability boundary in $(S, \alpha)$ space; equivalently, in $(y, x)$ space the unstable zone shrinks toward larger plasma radius. As a result, the value for the boundary layer position $x_1$ is increased and $H_{\rm crit}$ decreases accordingly. Shown in Fig. 8 is a plot of the numerically obtained values of $H_{\rm crit}$ versus $S_m$, with $\chi_{\rm max} = 20$, for a flux-conserving equilibrium. As expected, the value for $H_{\rm crit}$ is seen to decrease as the value of $S_m$ is increased.

# 5 Power Threshold Estimate

Having derived the threshold for the numerical quantity $H$, we now proceed to calculate the corresponding power. Obviously, any such estimate depends on what type of confinement scaling is taken to be dominant in the stable regime, how large an enhancement factor is assumed to be produced by the unstable ballooning modes, and what the size of the unstable region is in parameter space.

As a useful point of comparison, we apply our results to the Second Regime Experiment (SRX), a large-aspect-ratio tokamak that has been proposed at Columbia University [11,20]. Recently, Sabbagh *et al.* [11] have coupled the two-dimensional PEST equilibrium and stability code with the flux-surface averaged BALDUR transport code and have numerically studied the time evolution of a large-aspect-ratio tokamak plasma under the influence of neutral beam heating. Using neoclassical diffusion augmented by the Tang model [21] for anomalous transport (which is comparable to L-mode transport scaling) in the ballooning stable regime and enhancing it by a factor of ten in the unstable regime (which brings it up

to the local Bohm diffusion level), they found that the application of approximately 2.6 MW of beam heating is sufficient to power the SRX plasma into a second-stable configuration. The tokamak parameters in this case were $R = 1.5\,\mathrm{m}$, $a = 0.17\,\mathrm{m}$, $B = 1.0\,\mathrm{T}$, and $q_a = 4.0$.

Accordingly, with our model, we incorporate Goldston L-mode confinement scaling [22] (i.e., $\tau_E \approx P^{-0.50}$), take $\chi_{\max} = 10$, and select the parameters $S_m = 0.8$, $\overline{\alpha}_1 = 1.1$, and $\overline{\alpha}_2 = 2.7$, which approximately correspond to the simulation of Ref. [11]. Then, our analytic result given in Eq. (41), in the limit of $\lambda \to 0$, yields $H_{\mathrm{crit}} = H(x_{1,\max} = 0.73) = 20.3$, which would predict $P_{\mathrm{crit}} = 7.0\,\mathrm{MW}$. This number is reasonably near to the 2.6 MW of the SRX simulation [11], considering how many simplifications have been made in our model. In particular, it should be noted that the SRX simulation employed current programming by means of off-axis neutral beam heating; this reduces the current density near the magnetic axis, which increases $q_0$. Consequently, the size of the unstable region shrinks in time during the simulation, and less power is required for second stability access. Some other differences with our theoretical treatment are that the simulation incorporates particle diffusion; applies a package that combines multiple transport models; and takes the transport enhancement to be uniform throughout the unstable region.

Finally, we observe that the power levels estimated either with our theory or in the simulations of Ref. [11] need to be applied only for a relatively brief time interval. Shown in Fig. 9 is our calculation of the time $\Delta t_c$ (normalized) required for the plasma to go through the ballooning unstable zone. The parameters in Fig. 9 are $c_1 = 0.8$, $c_2 = 0.4$, $S_m = 0.8$, $\lambda = 2.5 \times 10^{-2}$, and $\chi_{\max} = 20$. We observe that the time $\Delta t_c$ decreases very rapidly with increasing power $H$. Approximately one energy confinement time is found to be required for access when the power is about 30% higher than the critical power value. (Of course, more time passes before the solution eventually settles down to a truly time-independent equilibrium.)

# 6 Concluding Remarks

We have numerically and analytically obtained the scalings for the auxiliary heating power required to access second stability as a function of the magnitude of the instability-induced anomalous thermal conductivity, for both flux-conserving tokamaks and flux non-conserving tokamaks.

Even though this theory for dynamical access to second stability predicts a large pressure gradient and a threshold in power, we do not claim it as an explanation for the L-mode to H-mode transition observed in auxiliary heated tokamaks. However, the application of this type of transport treatment to equilibria that incorporate the effect of a separatrix on ballooning modes, such as have been considered by Bishop [23], could be useful. If the present calculation were repeated in a divertor geometry, it might be expected that the threshold power for accessing high-beta stability would be reduced, since shear stabilization would be strong near the plasma edge.

Also, we distinguish between our globally second-stable, time asymptotic solution and a "locally" second-stable profile that has been recently described by Seki *et al.* [24]. In the latter, the pressure is strongly peaked near the magnetic axis, but relaxes to a flat, first-stable configuration for large values of the minor radius. (This sort of profile would appear to be susceptible to unstable moderate-mode-number infernal modes [25].) In contrast, our solution lies above the second stability limit at the edge of the plasma.

It should be pointed out that the power requirements for access to second stability tend to favor small machines with large aspect ratios. For example, with Goldston L-mode confinement [22], the threshold power scales as $P_{\rm aux} \propto \chi_{\rm max}^{1.0}\, a^{1.2}\, B^{2.0}\, q_a^{-2.0} (R/a)^{-1.5}$. Thus, estimates similar to that of Sec. 5, but applied to the proposed Compact Ignition Tokamak (CIT) and the International Thermonuclear Experimental Reactor (ITER) would tend to indicate unreasonably high power levels, simply because these devices are not designed to exploit second

stability.

Finally, we again note that our simple transport/stability model appears to give results that are both qualitatively and quantitatively in reasonable agreement with more sophisticated computational results. This correlation tends to bolster the viability of a large-aspect-ratio tokamak experiment designed to explore the second stability regime.

# Acknowledgments

Useful discussions with J. Hogan, T. Tuda, A. Bondeson, G.-S. Lee, T. Taniuti, and V. Demchenko are gratefully acknowledged. The authors especially thank S. Sabbagh, M. Hughes, and G. Navratil for sharing their results before publication. The work was supported by the U.S. Department of Energy under Contract No. DE-FG05-80ET-53088.

# References


1. ROSENBLUTH, M.N., TSAI, S.T., VAN DAM, J.W., ENGQUIST, M.G., Phys. Rev. Lett. **51** (1983) 1967.

2. MILLER, R.L., MOORE, R.W., Phys. Rev. Lett. **43** (1979) 765.

3. CHANCE, M.S., JARDIN, S.C., STIX, T.H., Phys. Rev. Lett. **51** (1983) 1963.

4. COPPI, B., CREW, G.B., RAMOS, J.J., Comments on Plasma Physics and Controlled Fusion **8** (1983) 11.

5. CONNOR, J.W., TAYLOR, J.B., TURNER, M.F., Nucl. Fusion **24** (1984) 642.

6. FU, G.Y., VAN DAM, J.W., J. Plasma Phys. **39** (1988) 11.

7. DEMCHENKO, V.V., FU, G.Y., VAN DAM, J.W., Phys. Fluids **31** (1988) 213.

8. FU, G.Y., VAN DAM, J.W, ROSENBLUTH, M.N., in Theory of Fusion Plasmas (Proceedings of the Workshop, Varenna, Italy, 1987) (BONDESON, A, SINDONI, E., TROYON, F., Eds.), Editrice Compositori, Bologna (1988) 153.

9. AZUMI, M., TSUNEMATSU, T., ITOH, K., TUDA, T., KURITA, G., TAKEDA, T., TAKIZUKA, T., TOKUDA, S., MATSUURA, T., TANAKA, Y., INOUE, S., TANAKA, M., in Plasma Physics and Controlled Nuclear Fusion Research 1980 (Proc. 8th Int. Conf. Brussels, 1980), Vol. 1, IAEA, Vienna (1981) 293.

10. TUDA, T., AZUMI, M., KURITA, G., Annual Controlled Fusion Theory Conference (Austin, Texas, 8-10 April 1981), Paper 1C6.

11. SABBAGH, S.A., HUGHES, M.H., PHILLIPS, M.W., TODD, A.M.M., NAVRATIL, G.A., Transition to the second region of ideal MHD stability, to be published in Nucl. Fusion.

12. RICHTMEYER, R.D., MORTON, K.W., Difference Methods for Initial-Value Problems, 2nd Ed., Interscience, New York (1967), Chap. 12 and references therein.

13. PASSOT, T., POUQUET, A., J. Comp. Phys. **75** (1988) 300.

14. STRAUSS, H.R., Phys. Fluids **28** (1985) 2786.

15. HOGAN, J.T., Bull. Am. Phys. Soc. **31** (1986) 1548.

16. LEE, G.S., private communication.

17. CARRERAS, B.A., Comments on Plasma Physics and Controlled Fusion **12** (1988) 35.

18. SAGDEEV, R.Z., in Reviews of Plasma Physics, Vol. 4 (LEONTOVICH, M.A., Ed.), Consultants Bureau, New York (1986) 23.

19. See, e.g., TIDMAN, D.A., KRALL, N.A., Shock Waves in Collisionless Plasmas, Wiley-Interscience, New York (1971) and references therein.

20. NAVRATIL, G.A., MARSHALL, T.C., Comments on Plasma Physics and Controlled Fusion **10** (1986) 185.

21. TANG, W.M., in Plasma Physics and Controlled Nuclear Fusion Research 1986 (Proc. 11th Int. Conf. Kyoto, 1986), Vol. 1, IAEA, Vienna (1987) 337; Nucl. Fusion **27** (1987) 2001.

22. GOLDSTON, R.J., Plasma Phys. Controlled Nucl. Fusion **26** (1984) 87.

23. BISHOP, C.M., Nucl. Fusion **26** (1986) 1063.

24. SEKI, S., TSUNEMATSU, T., AZUMI, M., MENOTO, T., Nucl. Fusion **27** (1987) 330.

25. MANICKAM, J., POMPHREY, N., TODD, A.M.M., Nucl. Fusion **27** (1987) 1461.

# Figure Captions

1. Evolution of the flux-conserving pressure gradient profile at successive times (a) $\tau = 0$, (b) $\tau = 0.1$, (c) $\tau = 0.15$, and (d) $\tau = 0.175$, relative to the ballooning stability boundary (dashed curve), for the parameters $H = 30$, $\chi_{\max} = 20$, $\lambda = 0.025$, $S_m = 0.8$, $c_1 = 0.8$, and $c_2 = 0.4$.

2. Flux-conserving profile evolution viewed in terms of the $S - \alpha$ variables, relative to the ballooning stability boundary (dashed curve), for the same parameters as in Fig. 1 except $H = 25$.

3. Steady-state pressure gradient profile for $H = 21$, just below the critical value $H_{\text{crit}} = 21.5$; other parameters as in Fig. 1.

4. Numerical results for the critical heating power $H_{\text{crit}}$ as a function of the transport enhancement factor $\chi_{\max}$, for a non- flux-conserving tokamak plasma ($S_m = 0.8$, $c_1 = 0.8$, $c_2 = 0.4$, and $\lambda = 2 \times 10^{-4}\chi_{\max}$).

5. Quasi-potential $V(y)$ for several values of the power $H$; other parameters as in Fig. 1.

6. Steady-state heating power $H(x_1)$ as a function of the boundary layer location $x_1$, for the parameters of Fig. 1, with the $\lambda = 0$ limit shown as a dashed curve.

7. Comparison of the numerical results for $H_{\text{crit}}$ versus $\chi_{\max}$, with the analytical results from the edge quasi-potential analysis and the boundary layer analysis (other parameters as in Fig. 1).

8. Critical power $H_{\text{crit}}$ as a function of the minimum unstable shear $S_m$ (other parameters as in Fig. 1).

9. Time $\Delta t_c$ required for a flux-conserving plasma to go through the ballooning unstable zone as a function of the applied power $H$ (other parameters as in Fig. 1).

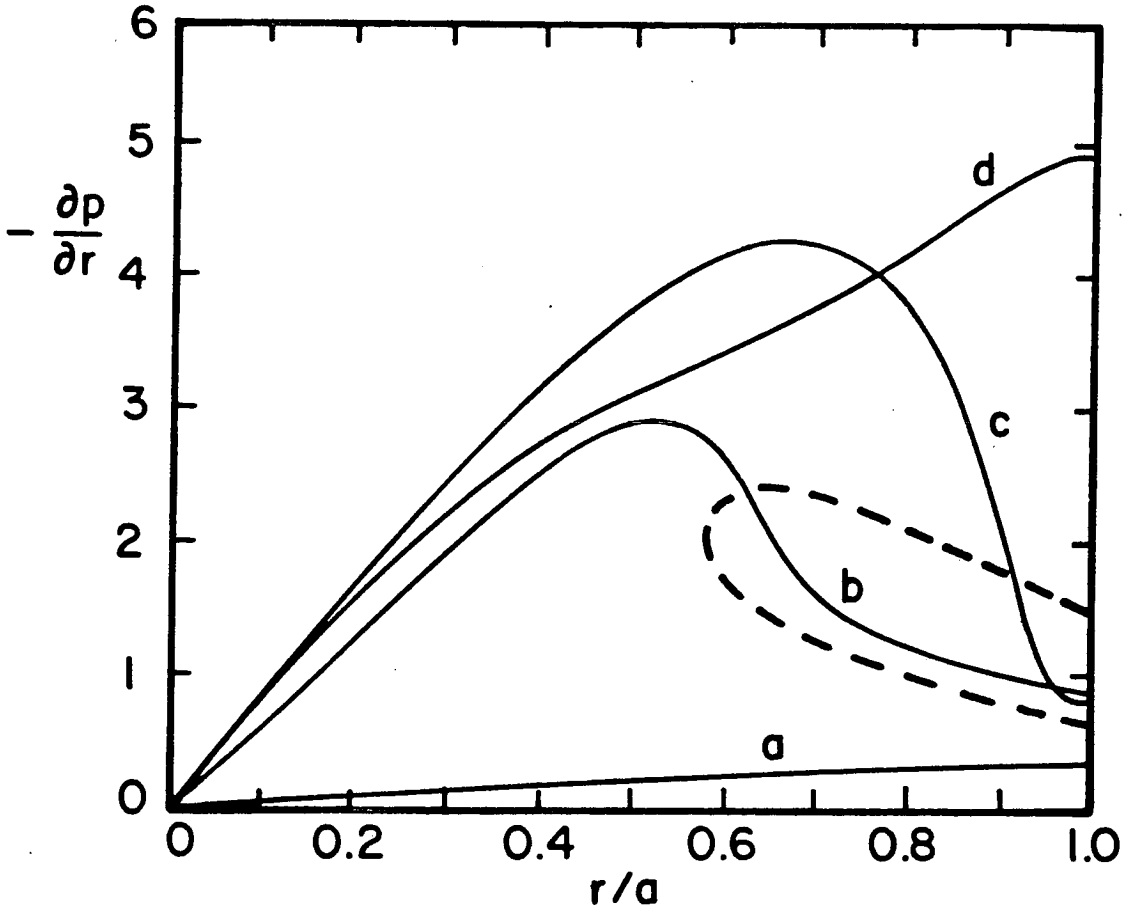


Fig. 1

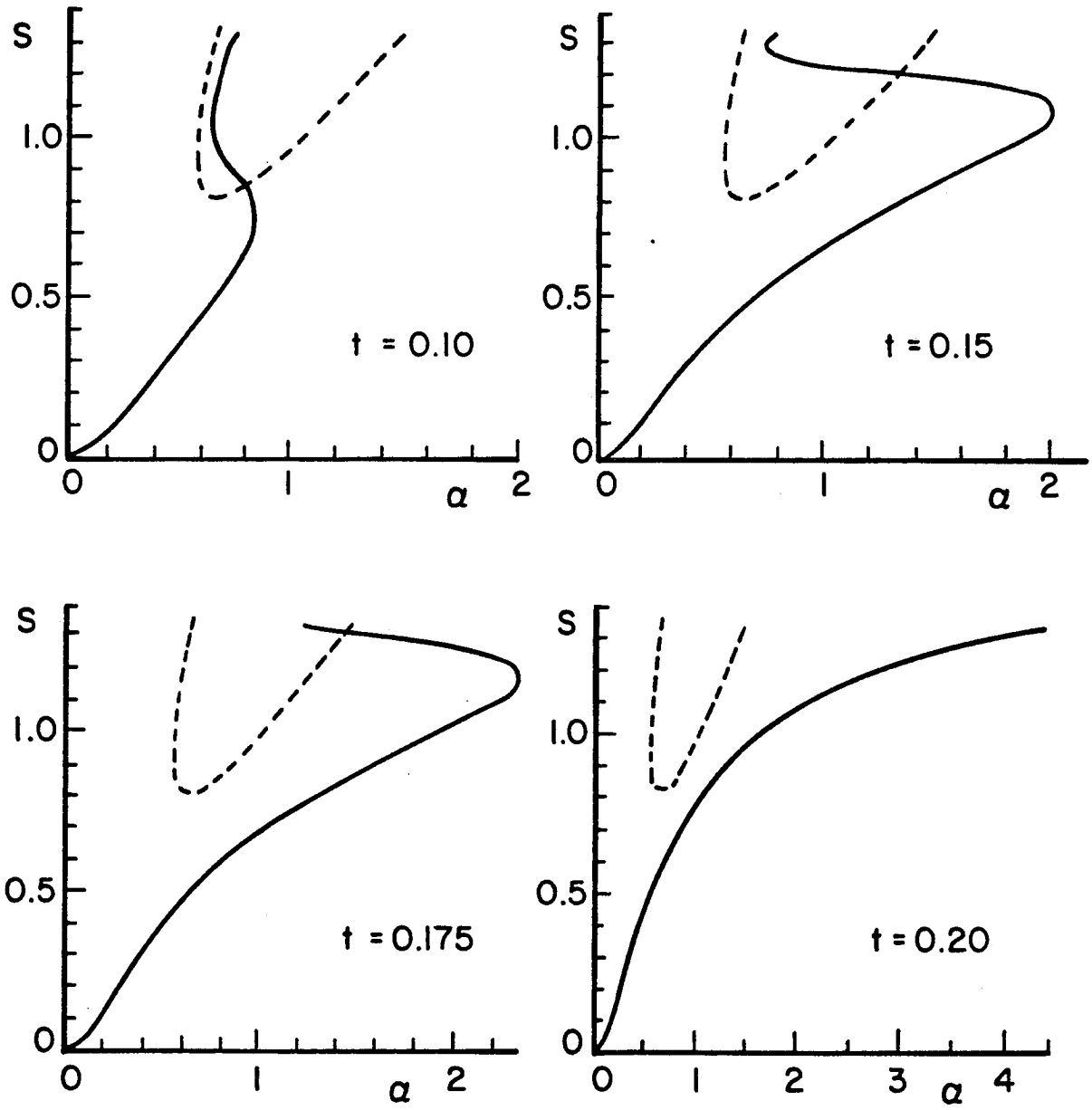
S
1.0
0.5
0
t = 0.10
0
1
α
2
S
1.0
0.5
0
t = 0.15
0
1
α
2
S
1.0
0.5
0
t = 0.175
0
1
α
2
S
1.0
0.5
0
t = 0.20
0
1
2
3
α
4

Fig. 2

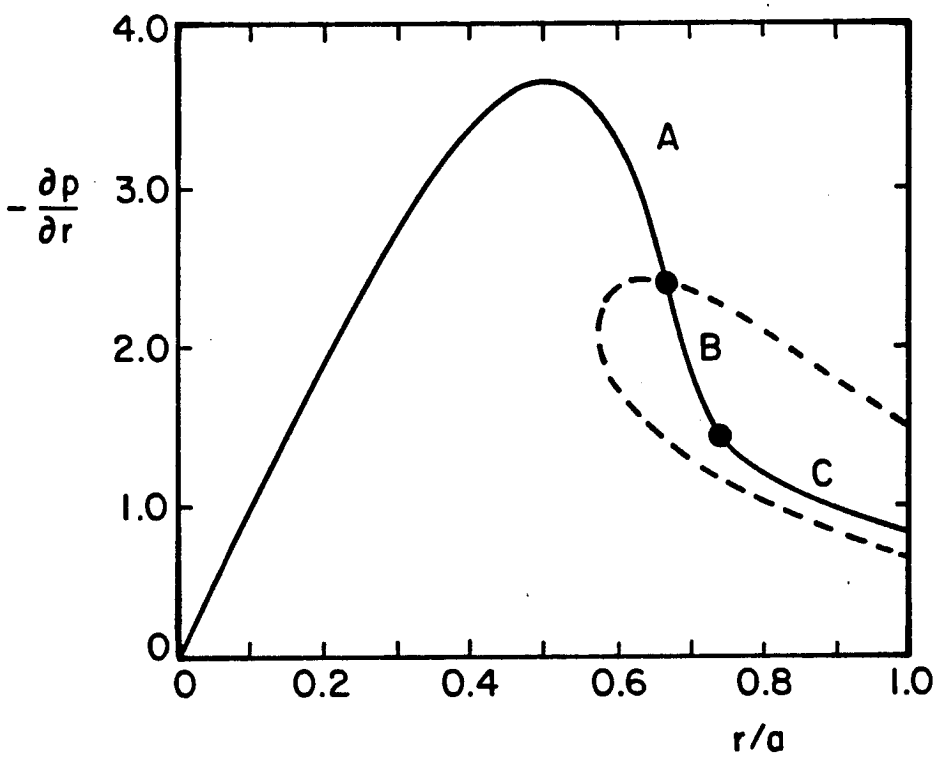


Fig. 3

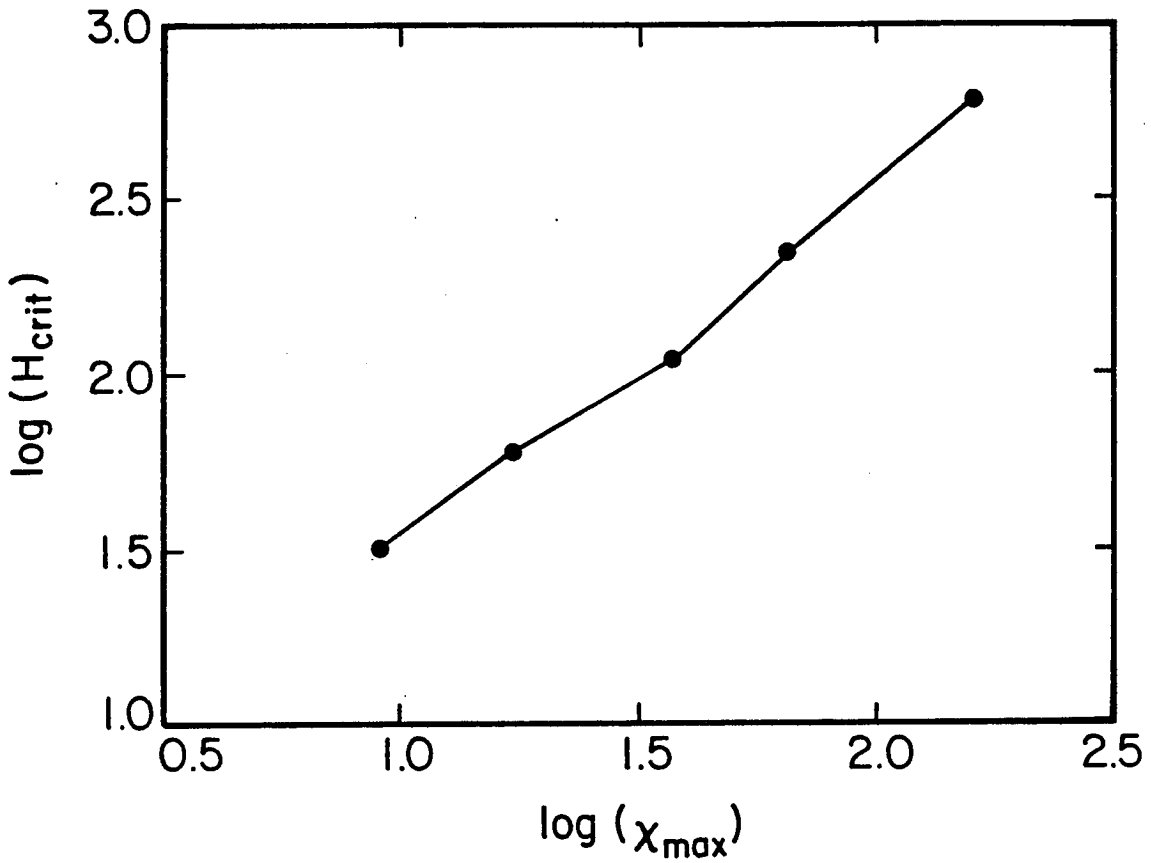


Fig. 4

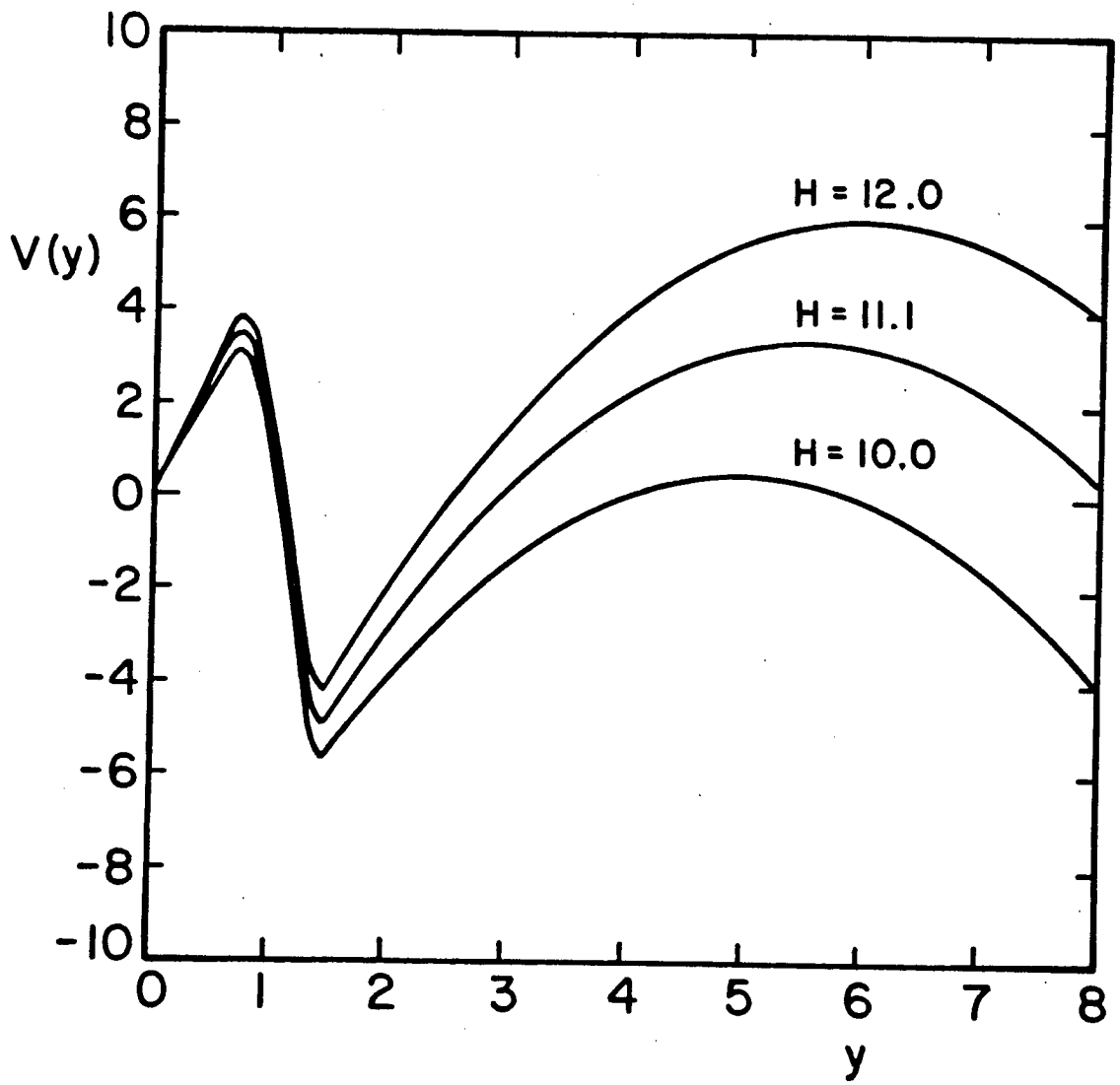


Fig. 5

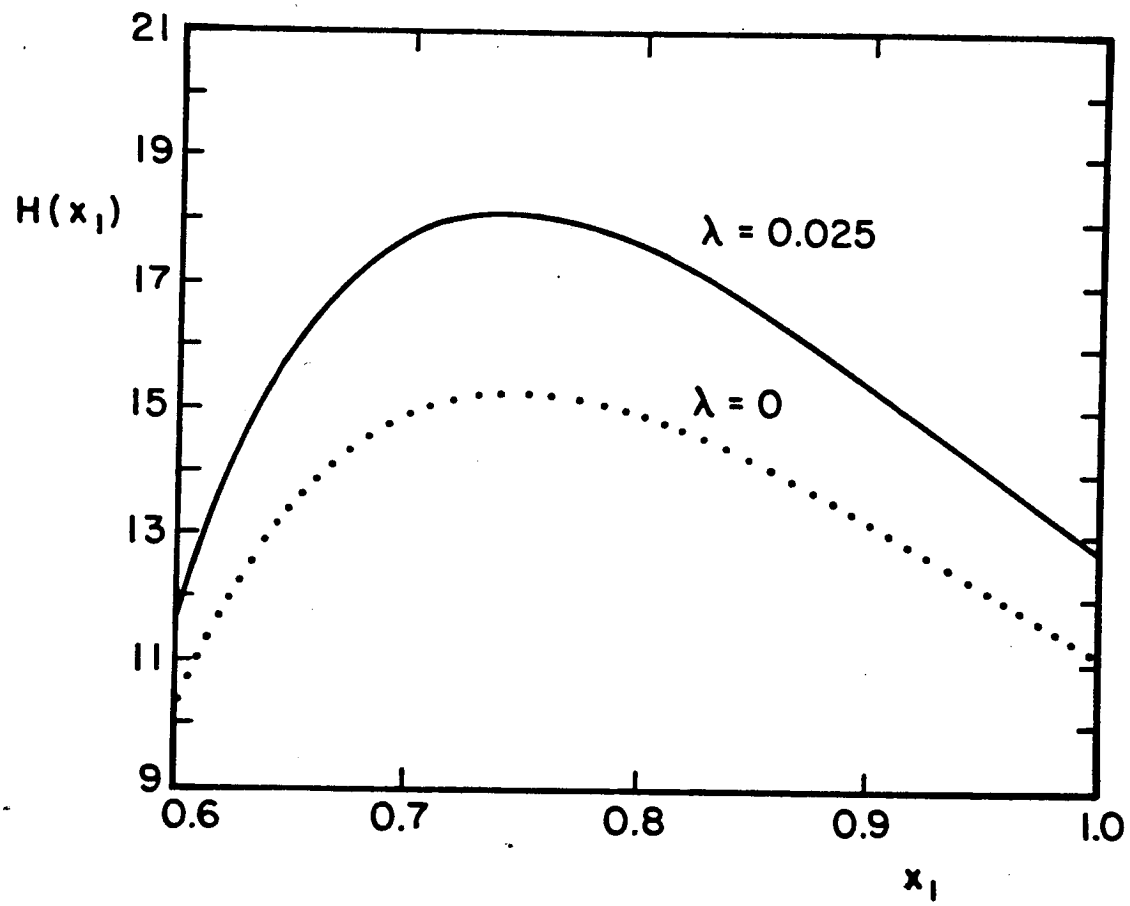


Fig. 6

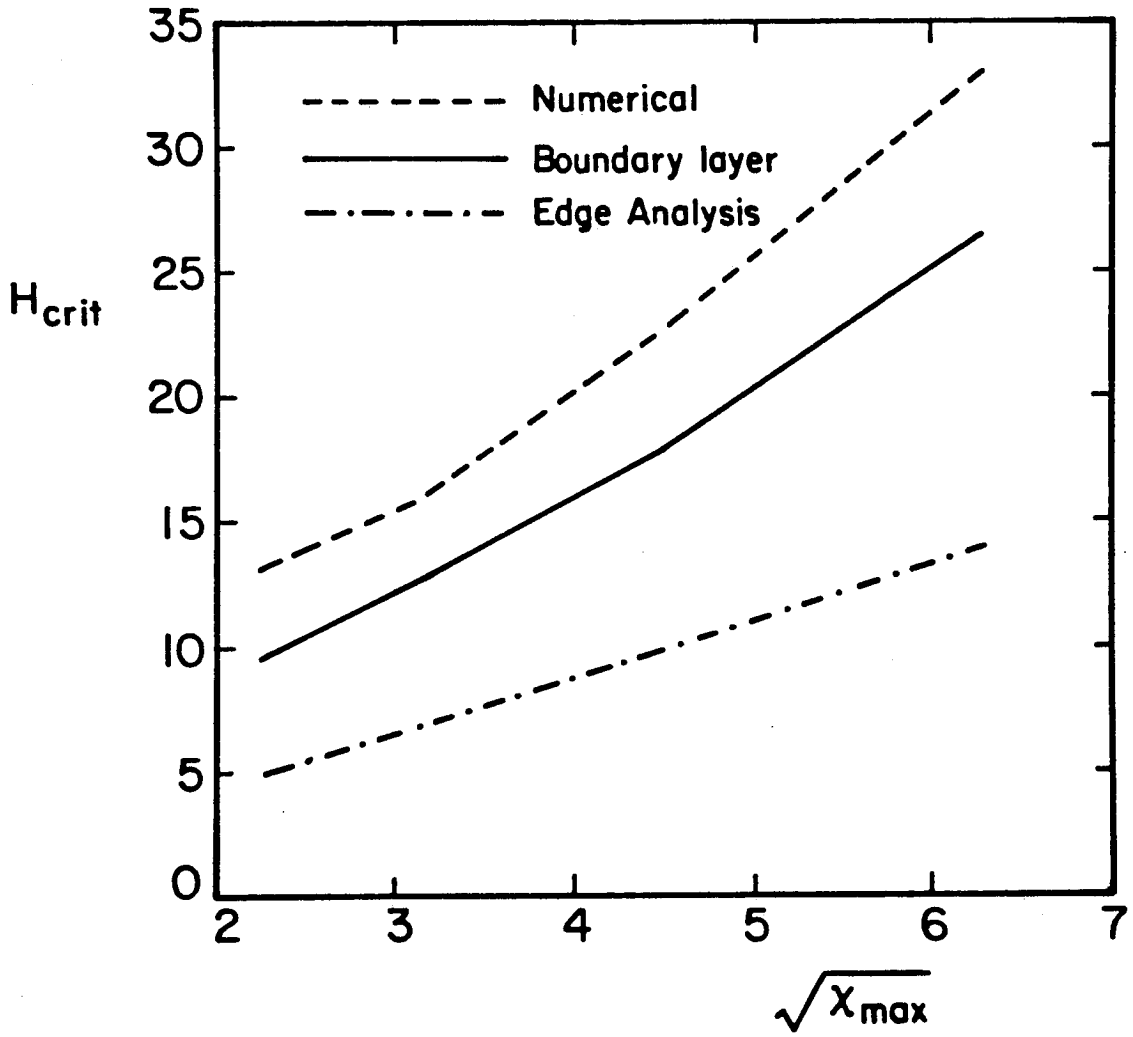
35
30
25
20
15
10
5
0
2
3
4
5
6
7
Numerical
Boundary layer
Edge Analysis
$H_{crit}$
$\sqrt{\chi_{max}}$

Fig. 7

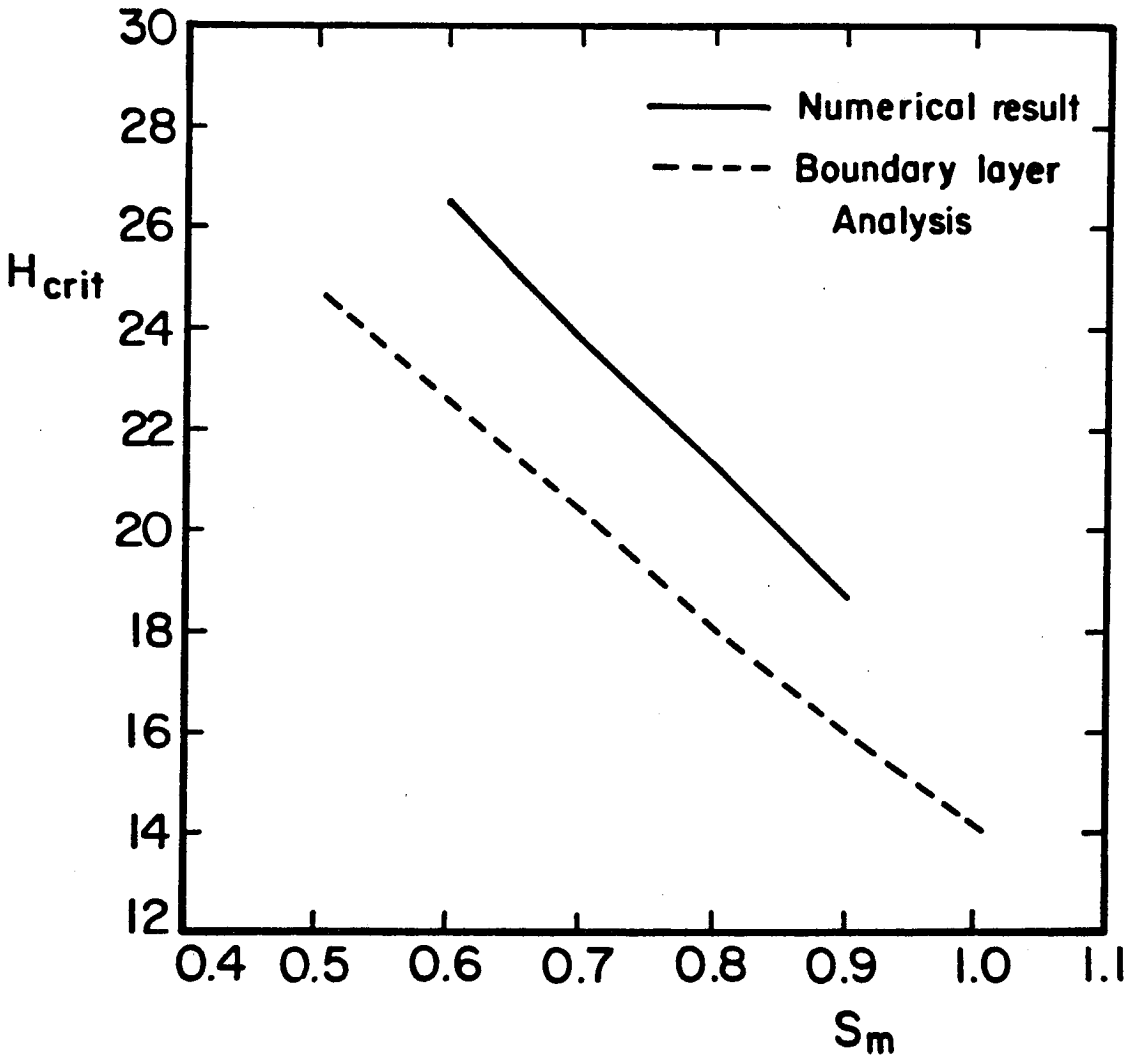
30
28
26
24
22
20
18
16
14
12
$H_{crit}$
0.4
0.5
0.6
0.7
0.8
0.9
1.0
1.1
$S_m$
Numerical result
Boundary layer
Analysis

Fig. 8

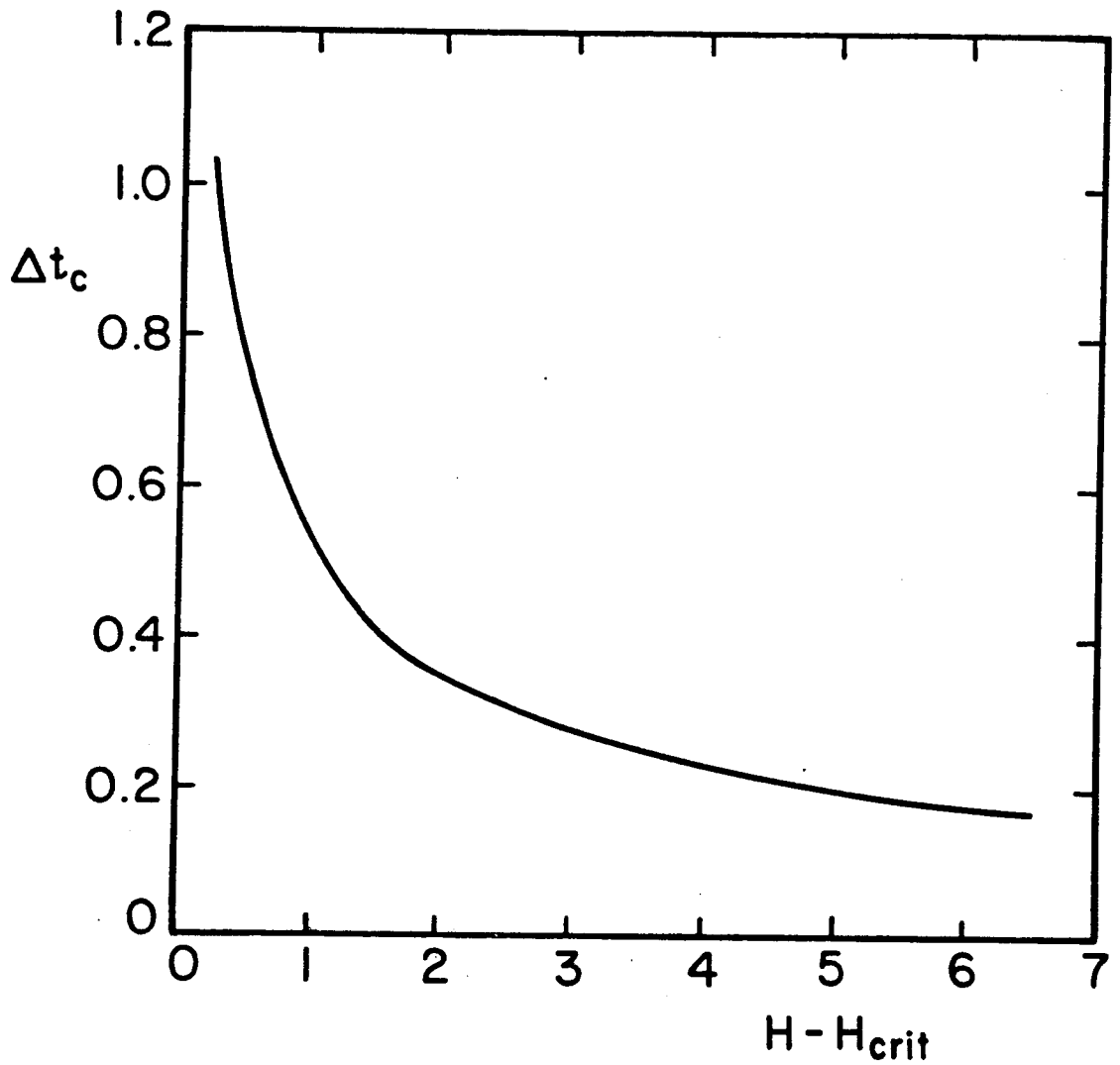


Fig. 9